Research Article | Vol. 31, No. 21 / 9 Oct 2023 / Optics Express 34264
Optics EXPRESS

On the error performance and channel capacity of a uniquely decodable coded FSO system over Malaga turbulence with pointing errors

YA-TIAN LI,[1,*] TIAN-WEN GENG,[1] AND SHI-JIE GAO[1,2]

[1] Changchun Institute of Optics, Fine Mechanics and Physics, Chinese Academy of Sciences, Changchun 130033, China
[2] University of Chinese Academy of Sciences, Beijing 100049, China
[*] yt_li@ciomp.ac.cn

Abstract: Our previous work has proved that the uniquely decodable code (UDC) has the ability of enhancing the throughput of a free space optical communication (FSO) system. This paper quantitatively analyzes the error performance and channel capacity of the UDC-FSO system under Malaga turbulence and pointing errors. We first propose the minimum distance of the superimposed patterns (MDSP) approximation to reveal the universal symbol error rate (SER) for UDC-FSO systems. A closed form expression of SER is further deduced for a special case of 2 TXs. Based on the deduced SER, the upper and lower bounds of bit error rate (BER) can be obtained. Additionally, the discrete channel capacity of the UDC-FSO system is defined and deduced according to different superposition patterns, as well as the channel capacity gain. Both simulation and experiment verify the accuracy of the MDSP and SER's expressions. It's also discovered that the channel capacity of the UDC-FSO system is superior to the conventional end-to-end (E2E) link, where maximal channel capacity is limited by the UDC codebooks.

1. Introduction

1.1. Background and related works

Free space optics (FSO) combines the advantages of wireless and fiber optic communication, which has numerous benefits such as high communication rate, high capacity, confidentiality, anti-electromagnetic interference [1–3]. Recently, National Aeronautics and Space Administration (NASA) has deployed and realized a 200 Gbps laser communication link from low earth orbit (LEO) satellites to the ground [4], which means the research of end-to-end (E2E) link has entered a new milestone. Driven by space-air-ground integrated network (SAGIN), the number of data nodes increases and the amount of data grows in a massive way. A more practical scenario is the information transfer between multiple nodes [5]. Therefore, how to further enhance the channel capacity of multi-node systems becomes a topic worthy of study.

Multiplexing technique is one of the most direct ways to enhance channel capacity. It introduces additional one- or multi-dimensional degrees of freedom, which brings about throughput improvement by increasing the number of available channels. [6] utilizes the polarization division multiplexing (PDM) in a full-duplex hybrid optical link with 40 Gbit/s. [7] demonstrates and analyzes diffractal spatial multiplexing schemes for communication with roving transceivers. Multicolor series connection micro-LED (light emitting diode) arrays are employed by wavelength division multiplexing in [8], where the achievable data rates of 400-, 451-, 509-, and 556-nm micro-LED arrays are 5.71, 4.86, 4.39, and 0.82 Gbps, respectively. [9] integrates mode division multiplexing (MDM) in a few-mode fiber (FMF) to improve density and efficiency, as well as interconnection capacity. Two-level laser diode (LD) based color-shift-keying orthogonal-frequency division-multiplexing (CSK-OFDM) signal are demonstrated for

#499764 https://doi.org/10.1364/OE.499764
Journal © 2023 Received 4 Jul 2023; revised 29 Aug 2023; accepted 18 Sep 2023; published 28 Sep 2023

Optics EXPRESS

the optical wireless communication (OWC) systems in [10], where the experiment achieves data rate of as high as 28.4 Gbit/s.

Although these multiplexing techniques enhance the channel capacity by introducing additional degrees of freedom, the utilized degrees of freedom are orthogonal and not fully exploited. It's inferred that the employment of non-orthogonal multiple access (NOMA) technique within the FSO systems will further enhance the channel capacity. Unfortunately, either the non-negativity of the power in on-off-keying (OOK) modulation or the non-existence of in-phase and quadrature (I/Q) components makes it impossible for the existing code domain (CD)-NOMA technique (such as sparse code multiple access (SCMA) [11]) in RF categories to be directly equipped in FSO systems. Though power domain NOMA (PD-NOMA) is another potential solution for visible light communications (VLC) [12], where OFDM technique is always utilized. Both the transceivers' architectures and the channel models are different from FSO systems in OOK schemes. Fortunately, unique decodable code (UDC) is an available form of implementing CD-NOMA [13,14]. Overall speaking, there are two main reasons for introducing UDC in FSO systems. The primary reason is that the power superposition of FSO signals in intensity modulation is mathematically consistent with the codeword superposition of UDC, since UDC is designed for multiple access adder channels. Moreover, UDC's non-orthogonal characteristic has the ability to further improve the channel capacity. It's also noticed that the UDC is different from the common channel coding technique. The former focuses on enhancing the effectiveness (increasing channel capacity), while the latter's purpose is improving the reliability (reducing BER), which is exploited to correct errors or recover erasure symbols in transmission.

Based on the above considerations, our previous work [15] proposes a UDC-FSO structure to increase the throughput for the first time, and proves that the received signals have uniquely decodable (UD) characteristics. The primary advantage of UDC-FSO is that the receiver can differentiate data from multiple data sources with only one processing unit, thus increasing the system throughput. It should be noted that UDC is not a multi-decimal system; on the contrary, the UDC can still be constructed under multi-decimal conditions [16,17]. What's more, common multiplexing techniques can be also employed in UDC-FSO systems to further increase the channel capacity.

1.2. Motivation and contribution

However, we do not give quantitative expressions in [15]. Once the closed expressions are obtained, the key factors affecting the system performance can be discovered accordingly. In turn, these key factors can be used as variables in subsequent studies to go for further optimization of the system performance. Therefore, the derivation of the expressions has theoretical significance and practical relevance.

Based on the above concerns, the primary work of this paper is to quantitatively analyze the error performance (including both symbol error rates (SER) and bit error rate (BER)) in the UDC-FSO system. Then the channel capacity of the UDC-FSO system is also studied. The main contributions are summarized as follows.

- Due to the irregular superimposed patterns in UDC-FSO systems caused by the product of discrete codeword space and continuous channel space, the minimum distance of the superimposed patterns (MDSP) approximation is proposed. And equivalent experiments are built to verify the effectiveness of MDSP.
- Based on the proposed MDSP approximation, the universal SER of a maximum likelihood (ML)-based soft-judgment receiver is derived. On the basis of SER, both the upper and lower bounds of BER are analyzed. Besides, the closed SER is derived for 2 TXs as an example. The accuracy of derived expressions is further verified by simulations for 2 TXs and 3 TXs cases.

Optics EXPRESS

- This paper analyzes the discrete channel capacity and the channel capacity gain based on entropy theory, which aims to describe the transmission effectiveness of the UDC-FSO system over traditional E2E FSO system.

1.3. Main differences from our previous work

Although both this paper and our previous work [15] focus on the M-to-1 UDC-FSO system, the main differences are summarized in Table 1. The most significant difference between this paper and [15] is that this paper performs a theoretical derivation after proposing the MDSP approximation, where the universal SER, closed-form SER for 2 TXs, bounds for BER are derived, while the previous work [15] only demonstrates the simulation and experimental results. It's found that the minimum distance $d_{\min}$ of the superimposed patterns is the core factor affecting both the SER and the channel capacity, which implies that future optimization of the UDC-FSO system may start from optimizing $d_{\min}$.

Table 1. Main differences between this paper and our previous work [15]

	This Paper	[15]
Theoretical Expressions	Universal SER, Closed-form SER for 2 TXs, Bounds for BER	-
Error Performance	SER, BER, conditional SER	SER only
Effectiveness Metrics	Discrete channel capacity based on entropy theory	Throughput (number of bits correctly transmitted per unit time)
Gain	Channel capacity gain	Throughput gain
Turbulent Model	Malaga	Gamma-Gamma

Besides, there are four other differences between this paper and [15]. This paper analyses both BER and SER, while [15] only studies the SER. Moreover, in terms of depicting the transmission effectiveness, we define and calculate the discrete channel capacity of a UDC-FSO system based on the information theory, which is more universal than the throughput discussed in [15]. The next difference is that in describing the gain in transmission effectiveness, channel capacity gain is studied in this paper, whereas throughput gain is analyzed in [15]. Additionally, there is a difference in channel models. Our previous work [15] has modeled the atmospheric turbulence as a Gamma-Gamma distribution, while this paper utilizes a more generalized Malaga distribution.

The remainder of this paper is organized as follows. Section 2 briefly depicts the system architecture and channel model. Section 3.1 presents the MDSP approximation and obtains the universal SER and bounds for BER. Section 3.2 derives the closed expression of 2 TXs' SER based on MDSP. Section 3.3 then reveals the channel capacity, as well as the channel capacity gain. The numerical results are furnished in Sec. 4. Finally, the conclusions of this paper are summarized in Sec. 5. For ease of reading, definitions of the main variables are summarized in Table 2.

Optics EXPRESS

Table 2. Definition of main variables

Symbol	Definition	Symbol	Definition
M	Number of TXs	ψ_i	i-th superimposed pattern
N_M	Number of superimposed patterns	κ_{ij}	Distance between ψ_i and ψ_j
P_s (P_b)	Symbol (Bit) error rate	$\mathbb{C}$	Total UDC codebook
$P(\psi_i)$	Prior probability of ψ_i	$\mathbb{C}_m$	m-th TX's UDC set
$P\left(\psi_j\|\psi_i\right)$	Conditional probability of judging ψ_i into ψ_j	C^{UDC} (C^{E2E})	Discrete channel capacity for UDC -FSO (or E2E FSO) systems
$\mathbf{c}_m^k$	m-th TX's k-th UDC codeword	$\mathcal{D}$	Set of distance pairs
$d_{\min}$	Smallest distance of $\{\psi_i\}_i$	$\mathcal{D}_c$	Set of candidates for $d_{\min}$
$\mathbf{x}_m^k$	Source data for m-th TX in k-th codeword	$\mathcal{G}_{\mathrm{UDC}}$	Channel capacity gain of UDC-FSO over E2E links
$\mathbf{y}^k$	Receiver's photocurrent in k-th codeword	$\mathbf{P}$	Transition probability matrix of a UDC-FSO system
$\|\bullet\|$	Number of elements in $\bullet$	$\hat{\bullet}$	Judgment result for $\bullet$

2. System model

Before depicting the system model, let's review the concept of UDC. According to [13–15], the UDC sets are first designed for the adder channel. $\mathbb{C} = \{\mathbb{C}_m\}$ can be defined as the UDC codebook consisting of any arbitrary m-th TX's UDC set $\mathbb{C}_m$, if and only if all the codewords $\mathbf{u}_m, \mathbf{v}_m \in \mathbb{C}_m$ satisfy $\sum_{m=1}^{M} \mathbf{u}_m \neq \sum_{m=1}^{M} \mathbf{v}_m$ where the set $\{\mathbf{u}_m\}$ is different from the set $\{\mathbf{v}_m\}$, i.e., $\{\mathbf{u}_m\} \neq \{\mathbf{v}_m\}$. Our previous work [15] proposes the UDC-FSO structure and proves that the received fading signals maintain UD characteristics.

On the basis of [15], M TXs send data simultaneously to a single RX in the UDC-FSO system, as shown in the left part of Fig. 1. For the m-th TX to transmit any arbitrary k-th codeword, the source data $\mathbf{x}_m^k$ are first encoded to UDC codeword $\mathbf{c}_m^k$, which is chosen from the m-th UDC set $\mathbb{C}_m$. For UDC codewords with length n, n time slots (TSs) are costed to send a complete codeword. The received photocurrent $\mathbf{y}^k$ can be expressed as

$$\mathbf{y}^k = \eta \sum\nolimits_{m=1}^{M} h_m^k \cdot \mathbf{c}_m^k + \mathbf{n}^k, \tag{1}$$

where η stands for the photo-electric conversion ratio. $\mathbf{n}^k$ represents the additive white Gaussian noise (AWGN) with zero-mean and variance equal to σ_n^2. In UDC-FSO systems, $\mathbf{y}^k$ is defined as the "superimposed symbols", while $\eta \sum_{m=1}^{M} h_m^k \cdot \mathbf{c}_m^k$ can be referred to as "superimposed patterns". Both the "superimposed symbols" and "superimposed patterns" are n-tuple vectors.

Different from the Gamma-Gamma channel in [15], the Malaga turbulence with pointing errors is considered in this paper, which is more generalizable. Besides, the composite FSO channel gain also includes the path loss h_l and misalignment loss. The probability distribution function (PDF) and cumulative distribution function (CDF) are furnished below [18,19]. It is assumed that the channel gains $\{h_m^k\}$ have the same distribution.

$$f_h(h) = \frac{\xi^2 A}{2h} \sum_{m=1}^{\beta} b_m \cdot \mathbf{G}_{1,3}^{3,0}\left[\frac{\alpha\beta}{(g\beta+\Omega')} \frac{h}{h_l A_0} \middle| \begin{matrix} \xi^2+1 \\ \xi^2, \alpha, m \end{matrix} \right], \tag{2}$$

$$F_h(h) = \frac{\xi^2 A}{2} \sum_{m=1}^{\beta} b_m \cdot \mathbf{G}_{2,4}^{3,1}\left[\frac{\alpha\beta}{(g\beta+\Omega')} \frac{h}{h_l A_0} \middle| \begin{matrix} 1, \xi^2+1 \\ \xi^2, \alpha, m, 0 \end{matrix} \right], \tag{3}$$

Optics EXPRESS

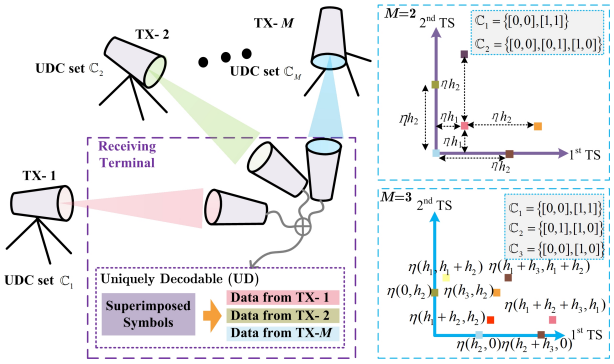

Fig. 1. The UDC-FSO system and the superimposed patterns.

where $\mathbf{G}_{1,3}^{3,0}(\cdot)$ stands for the Meijier'G function. α is the effective number of large-scale cells in scattering process, while β is the amount of fading parameters. g denotes the average power of the scattering component received by off-axis eddies. Ω' represents the average power from the coherent contributions. A and b_m are defined as $\frac{2\alpha^{\alpha/2}}{g^{1+\alpha/2}\Gamma(\alpha)}(g\beta/g\beta+\Omega')^{\beta+\alpha/2}$ and $a_m[\alpha\beta/(g\beta+\Omega')]^{-(\alpha+m)/2}$, respectively. a_m is short for $\left(\frac{\beta-1}{m-1}\right)(g\beta+\Omega')^{1-m/2}/(m-1)!$ $\left(\Omega'/g\right)^{m-1}(\alpha/\beta)^{m/2}$. A_0 is a constant term that defines the pointing loss. ξ is the ratio between the receiver's equivalent beam radius and pointing error displacement standard deviation.

According to the right half of Fig. 1, it's clear that the superimposed patterns still maintain UD characteristics after passing through the fading channel (i.e., $\sum_{m=1}^{M} h_m^k \cdot \mathbf{v}_m \neq \sum_{m=1}^{M} h_m^k \cdot \mathbf{u}_m$ for $\{\mathbf{v}_m \in \mathbb{C}_m\} \neq \{\mathbf{u}_m \in \mathbb{C}_m\}$), which indicates that they can be adjudicated and demodulated. The receiver employs a soft-judgment. Then the codewords after decision are

$$\{\hat{\mathbf{c}}_m^k\} = \arg\min_{\{\mathbf{u}_m\}} \left\| \mathbf{y}^{\mathbf{k}} - \eta \sum_{m=1}^{M} h_m \cdot \mathbf{u}_m \right\|^2, \mathbf{u}_{\mathbf{m}} \in \mathbb{C}_m. \tag{4}$$

Then one can decode the message $\{\hat{\mathbf{x}}_x^k\}$ according to $\{\hat{\mathbf{c}}_m^k\}$ by the corresponding de-mapping method [15]. For brevity, the superscript k of the channel gains h_m^k are neglected during the following derivation.

3. Theoretical analysis

3.1. MDSP approximation, universal SER, bounds for BER

To obtain SER's expressions, it's common to delineate the judgment region according to the ML judgment criterion and then perform the integrations in each region. Taking the previously mentioned UDC codebook as an example, it's apparent from in the right part of Fig. 2 that the judgment region is irregular which infers that the integrations in these regions are complicated. Let alone the situation of larger M or longer codewords. Therefore, the MDSP approximation method is proposed in this paper so as to simplify the SER derivation process.

Recalling that there are $N_M = \prod_{m=1}^{M} |\mathbb{C}_m|$ possible superimposed patterns in each n TSs, where $|\bullet|$ denotes the numbers in set $\bullet$. The superimposed patterns can be labeled as ψ_i, $i = 1, 2, \ldots, N_M$. For any superimposed pattern, there are always $N_M - 1$ distance pairs. These distance pairs form a distance set $\mathcal{D} = \{\kappa_{ij} | 1 \leq i \leq j \leq N_M\}$ with $N_M \times (N_M - 1)/2$ elements due to the reciprocity of $\kappa_{ij} = \kappa_{ji}$, where κ_{ij} represents the distance between ψ_i and ψ_j the n-tuple space. As can be seen from Fig. 2, there are the 6 superimposed patterns $\psi_1, \psi_2, \ldots, \psi_6$. Combining the coordinates of all superimposed patterns in Fig. 1, the corresponding coordinates are $(0, 0)$, $(\eta h_2, 0)$, $(0, \eta h_2)$,

Optics EXPRESS

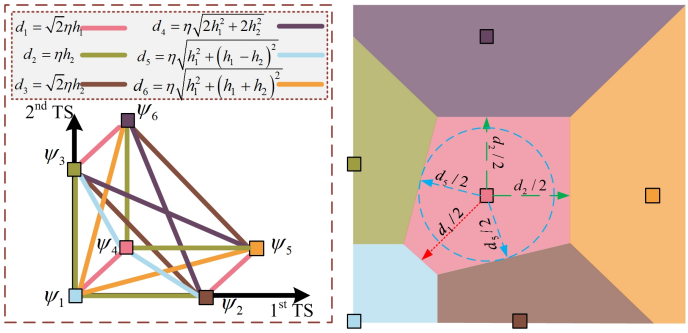

Fig. 2. Distances between superimposed patterns and judgement regions with $\mathbb{C}_1 = \{[0,0],[1,1]\}, \mathbb{C}_2 = \{[0,1],[1,0],[0,0]\}$.

$(\eta h_1, \eta h_1)$, $(\eta(h_1+h_2), \eta h_1)$, $(\eta h_1, \eta(h_1+h_2))$, respectively. The length of the line connecting the i-th and j-th superimposed patterns is the corresponding κ_{ij}.

Note that there may be duplicate elements in $\mathcal{D}$. To facilitate the description, $\mathcal{D}_c$ is defined as the set of candidates for $d_{\min}$, which can be obtained by removing duplicate elements in $\mathcal{D}$, whose smallest element is $d_{\min}$. To facilitate the understanding of abstract $\mathcal{D}$ and $\mathcal{D}_c$, we take the UDC codebook in Fig. 2 as an example. Following the above definition, $\mathcal{D}$ has $6 \times 5/2 = 15$ elements, i.e., $\mathcal{D} = \{\kappa_{12}, \kappa_{13}, \kappa_{14}, \kappa_{15}, \kappa_{16}, \kappa_{23}, \kappa_{24}, \kappa_{25}, \kappa_{26}, \kappa_{34}, \kappa_{35}, \kappa_{36}, \kappa_{45}, \kappa_{46}, \kappa_{56}\}$, where $\kappa_{14} = \kappa_{36} = \kappa_{25} = \sqrt{2}\eta h_1$, $\kappa_{13} = \kappa_{12} = \kappa_{45} = \kappa_{46} = \eta h_2$, $\kappa_{23} = \kappa_{56} = \sqrt{2}\eta h_2$, $\kappa_{35} = \kappa_{26} = \eta\sqrt{2h_1^2 + 2h_2^2}$, $\kappa_{34} = \kappa_{24} = \eta\sqrt{h_1^2 + (h_1 - h_2)^2}$, $\kappa_{15} = \kappa_{16} = \eta\sqrt{h_1^2 + (h_1 + h_2)^2}$. In this sequel, we can conclude that there will be 6 elements in $\mathcal{D}_c$ in this case, which can be labeled as $d_1, d_2, \ldots, d_6$ as shown in Fig. 2.

REMARK 1 *The SER P_s of a UDC-FSO system is dominantly affected by the minimum distance of the superimposed patterns. Based on all candidates of $d_{\min}$, the universal SER of a UDC-FSO system can be approximately calculated by*

$$P_s \approx \mathbb{E}\left[Q\left(\frac{d_{\min}}{2\sigma_n}\right)\right] = \sum_{d_q \in \mathcal{D}_c} P\left(d_{\min} = d_q\right)\mathbb{E}\left[Q\left(\frac{d_{\min}}{2\sigma_n}\right)\middle| d_{\min} = d_q\right], \tag{5}$$

where $Q(x) = \int_x^{+\infty} \frac{1}{\sqrt{2\pi}} \exp(-\frac{1}{2}t^2)dt$ denotes the Q-function.

PROOF *For the sake of consistency, the proof of* **REMARK** *1 can be found in the APPENDIX.* ■

It's noted that the MDSP approximation is independent of codeword length n. It may be assumed that ψ_{i_d} and ψ_{j_d} have a minimum distance $d_{\min}$. The physical meaning represented by **REMARK** 1 is that the SER can be calculated by $P(n_{eq} > d_{\min}/2)$. where n_{eq}^k represents the projection of the $\mathbf{n}^k$ on the line connecting ψ_{i_d} and ψ_{j_d}. For a better visualization, let's take $n = 2$ as an example. Suppose that θ represents the angle between the line connecting ψ_{i_d} to ψ_{j_d} and the horizontal axis, so the projection of the noise $\mathbf{n}^k = \left[n_1^k, n_2^k\right]$ on the line is $n_{eq}^k = n_1^k \cdot \cos\theta + n_2^k \cdot \sin\theta$, whose variance is equal to σ_n^2.

As can be obtained from **REMARK** 1, one can optimize the SER can by maximizing $d_{\min}$. It's also discovered that the UDC codebook $\mathbb{C}$ determines the overall shape of superimposed patterns, while the received power from different TX determines the amplitudes of superimposed patterns. In this sequel, $d_{\min}$ is influenced by both the discrete codeword space and continuous power space, which indicates UDC-FSO systems can be further optimized by codeword construction and power allocation.

Optics EXPRESS

To reveal the meaning of **REMARK** 1 more intuitively, we illustrate it graphically. In fact, it can be seen by **REMARK** 1 that we approximate the judgment region as a multidimensional spherical region with the radius of $d_{\min}/2$. Taking the middle superimposed pattern ψ_4 in Fig. 2 as an example, the true pentagonal judgment region is approximated as a circle.

Consider that each superimposed pattern contains $\log_2 N_M$ bits. Then, when there is any superimposed pattern ψ_i is judged as $\psi_j (1 \neq i \neq j \geq N_M)$, there will be at least 1 error bit and at most $\log_2 N_M$ error bits. Therefore, it is possible to obtain the upper and lower bounds for BER P_b in Eq. 6.

$$P_s/\log_2 N_M \leq P_b \leq P_s, \tag{6}$$

which can be verified in Sec. 4.

3.2. Special case for SER with $N = 2$

In this subsection, the closed SER for the case of 2 TXs is derived. Recalling that there are 15 distance pairs in $\mathcal{D}$ with $N_M = 6$, the elements in $\mathcal{D}$ can be divided into 6 kinds of distances namely $d_1, d_2, \ldots, d_6$, whose expressions are given in Fig. 2. In other words, there are 6 elements in $\mathcal{D}_c$. Among these 6 elements, we can find that d_3 is always larger than d_2, due to $d_3 = \sqrt{2}\eta h_2 > d_2 = \eta h_2$. In the similar way, both d_6 and d_4 are larger than d_1, which owes to the inequality deflation $d_6 = \eta\sqrt{h_1^2 + (h_1 + h_2)^2} > \eta\sqrt{h_1^2 + h_1^2} = d_1$ and $d_4 = \eta\sqrt{2h_1^2 + 2h_2^2} > \eta\sqrt{2h_1^2} = d_1$. As a result, there are only three candidates for $d_{\min}$, which are d_1, d_2 and d_5. That is to say, $P\left(d_{\min} = d_q\right) = 0$ for $q = 3, 4, 6$.

As previously described, the superposition patterns are related to the UDC codebook and the channel gains. Therefore, when the UDC codebook is determined, the superposition patterns are only affected by the channel gains. In other words, among the three candidates d_1, d_2, d_5, the smallest one is determined as $d_{\min}$ for different channel gains h_1 and h_2. Next, we will discuss three cases of d_1, d_2, d_5 being the minimum value, respectively. Firstly, let's consider the case $d_{\min} = d_1$, i.e., $d_1 < d_5$, $d_1 < d_2$. These two inequalities correspond to $h_1 < h_2/\sqrt{2}$ and $h_1 < \frac{1}{2}h_2$, respectively. After calculating the intersection in these two ranges, it can be seen that $d_{\min} = d_1$ when $h_2 > 2h_1$. Similarly, we can obtain that $d_{\min} = d_2$ (or d_5), if $h_2 < h_1$ (or $h_1 < h_2 < 2h_1$). As a result, the h_1-to-h_2 plane can be divided into three regions corresponding to $d_{\min} = d_1, d_2, d_5$, which are depicted in Fig. 3. The three regions are $h_2 > 2h_1$, $h_2 < h_1$, $h_1 < h_2 < 2h_1$, respectively. Corresponding to these three cases, the SER can be also divided into three parts,

$$P_s = P_s^{d_1} + P_s^{d_2} + P_s^{d_5}, \tag{7}$$

where $P_s^{d_q}$ denotes the probability $\mathbb{E}\left[Q\left(\frac{d_{\min}}{2\sigma_n}\right) | d_{\min} = d_q\right] \times P(d_{\min} = d_q)$ for $q = 1, 2, 5$.

Therefore, the next task is to derive $P_s^{d_q}$. According to the above definition, $P_s^{d_1}$ can be expressed as

$$P_s^{d_1} = \iint_{h_2 > 2h_1} Q\left(\frac{d_1}{2\sigma_n}\right) f_h(h_1) f_h(h_2)\, dh_1 dh_2. \tag{8}$$

Expanding this dual integral in Eq. 8, we can obtain

$$\begin{aligned} P_s^{d_1} &= \int_0^{+\infty} \underbrace{\int_{2h_1}^{+\infty} f_h(h_2)\, dh_2}_{1 - F_h(2h_1)} Q\left(\frac{\sqrt{2}\eta h_1}{2\sigma_n}\right) f_h(h_1) dh_1 \\ &= \int_0^{+\infty} \left[1 - F_h(2h_1)\right] Q\left(\frac{\sqrt{2}\eta h_1}{2\sigma_n}\right) f_h(h_1) dh_1. \end{aligned} \tag{9}$$

According to [20], $Q(x)$ can be approximated by $\frac{1}{12}e^{-x^2/2} + \frac{1}{4}e^{-2x^2/3}$. In the sequel, one can find that Eq. 8 satisfies the form of Hermite expansion, i.e., $\int_0^{\infty} g(x) \cdot e^{-x^2}\, \mathrm{d}x = \sum_{i=0} \omega_i g(x_i)$. x_i

Optics EXPRESS

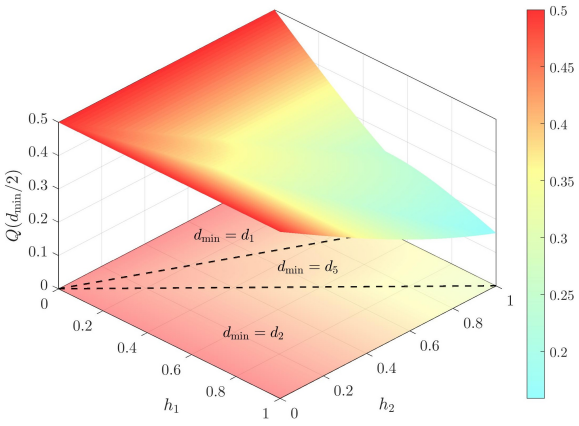

Fig. 3. Schematic diagram of $Q(d_{\min}/2)$ and $d_{\min}$ area division with $d_{\min} = d_1, d_2, d_5$.

and ω_i are the roots and the weights of Hermite polynomial. One can refer to the demo program in [21] to obtain x_i and ω_i. In the sequel, Eq. 8 can be transformed into Eq. 10,

$$P_s^{d_1} = \underbrace{\frac{\sigma_n}{6\eta}\sum_{i=1}^{N}\omega_i\left[f_h\left(\frac{2\sigma_n}{\eta}x_i\right) - f_h\left(\frac{4\sigma_n}{\eta}x_i\right)f_h\left(\frac{2\sigma_n}{\eta}x_i\right)\right]}_{P_{s,\text{part1}}^{d_1}} + \underbrace{\frac{\sqrt{3}\sigma_n}{4\eta}\sum_{i=1}^{N}\omega_i\left[f_h\left(\frac{\sqrt{3}\sigma_n}{\eta}x_i\right) - f_h\left(\frac{2\sqrt{3}\sigma_n}{\eta}x_i\right)f_h\left(\frac{\sqrt{3}\sigma_n}{\eta}x_i\right)\right]}_{P_{s,\text{part2}}^{d_1}}. \tag{10}$$

As can be observed from Eq. 10, $P_s^{d_1}$ can be divided into two parts $P_{s,\text{part1}}^{d_1}$ and $P_{s,\text{part2}}^{d_1}$ corresponding to the two lines within Eq. 10. After substituting Eqs. 2 and 3 into Eq. 10, $P_{s,\text{part1}}^{d_1}$ and $P_{s,\text{part2}}^{d_1}$ can be simplified as

$$P_{s,\text{part1}}^{d_1} = \frac{\xi^2 A}{24}\sum_{i=1}^{N}\frac{\omega_i}{x_i}\left[\sum_{m=1}^{\beta} b_m \mathbf{G}_{1,3}^{3,0}\left(\frac{2\alpha\beta\sigma_n x_i}{(g\beta+\Omega')\eta h_l A_0}\right) - \frac{\xi^2 A}{2}\sum_{m=1}^{\beta}\sum_{l=1}^{\beta} b_m b_l \mathbf{G}_{1,3}^{3,0}\left(\frac{2\alpha\beta\sigma_n x_i}{(g\beta+\Omega')\eta h_l A_0}\right)\mathbf{G}_{2,4}^{3,1}\left(\frac{4\alpha\beta\sigma_n x_i}{(g\beta+\Omega')\eta h_l A_0}\right)\right], \tag{11}$$

$$P_{s,\text{part2}}^{d_1} = \frac{\xi^2 A}{8}\sum_{i=1}^{N}\frac{\omega_i}{x_i}\left[\sum_{m=1}^{\beta} b_m \mathbf{G}_{1,3}^{3,0}\left(\frac{\sqrt{3}\alpha\beta\sigma_n x_i}{(g\beta+\Omega')\eta h_l A_0}\right) - \frac{\xi^2 A}{2}\sum_{m=1}^{\beta}\sum_{l=1}^{\beta} b_m b_l \mathbf{G}_{1,3}^{3,0}\left(\frac{\sqrt{3}\alpha\beta\sigma_n x_i}{(g\beta+\Omega')\eta h_l A_0}\right)\mathbf{G}_{2,4}^{3,1}\left(\frac{2\sqrt{3}\alpha\beta\sigma_n x_i}{(g\beta+\Omega')\eta h_l A_0}\right)\right], \tag{12}$$

where $\mathbf{G}_{1,3}^{3,0}(\bullet)$ and $\mathbf{G}_{2,4}^{3,1}(\bullet)$ are short for $\mathbf{G}_{1,3}^{3,0}\left(\bullet\middle|\begin{matrix}\xi^2+1\\ \xi^2,\alpha,m\end{matrix}\right)$ and $\mathbf{G}_{2,4}^{3,1}\left(\bullet\middle|\begin{matrix}1,\xi^2+1\\ \xi^2,\alpha,l,0\end{matrix}\right)$, respectively.

As can be seen from Eqs. 11 and 12, they both have similar forms. This is because the $P_{s,\text{part1}}^{d_1}$ and $P_{s,\text{part2}}^{d_1}$ are produced due to the approximation of the $Q(x)$ to the sum of two exponential

Optics EXPRESS

functions, and those two terms are very similar. Therefore, we can calculate the summation of Eqs. 11 and 12, which in turn gives us the expression for $P_s^{d_1}$,

$$\begin{aligned} P_s^{d_1} = & \frac{\xi^2 A}{24} \sum_{j=0}^{1} 3^j \sum_{i=1}^{N} \frac{\omega_i}{x_i} \left[\sum_{m=1}^{\beta} b_m \mathbf{G}_{1,3}^{3,0} \left(\frac{\left(\sqrt{3}/2\right)^j 2\alpha\beta\sigma_n x_i}{(g\beta+\Omega')\eta h_l A_0} \right) \right. \\ & \left. - \frac{\xi^2 A}{2} \sum_{m=1}^{\beta} \sum_{l=1}^{\beta} b_m b_l \mathbf{G}_{1,3}^{3,0} \left(\frac{\left(\sqrt{3}/2\right)^j 2\alpha\beta\sigma_n x_i}{(g\beta+\Omega')\eta h_l A_0} \right) \mathbf{G}_{2,4}^{3,1} \left(\frac{\left(\sqrt{3}/2\right)^j 4\alpha\beta\sigma_n x_i}{(g\beta+\Omega')\eta h_l A_0} \right) \right] \end{aligned} . \tag{13}$$

Similar to the derivation process with $P_s^{d_1}$, the expression of $P_s^{d_2}$ can be obtained as follows,

$$\begin{aligned} P_s^{d_2} &= \iint_{h_2<h_1} Q\left(\frac{d_2}{2\sigma_n}\right) f_h(h_1) f_h(h_2)\, dh_1 dh_2 \\ &= \int_0^{+\infty} \left[1 - F_h(h_2)\right] Q\left(\frac{\eta h_2}{2\sigma_n}\right) f_h(h_2) dh_2, \end{aligned} \tag{14}$$

which can be further simplified by Hermite expansion,

$$\begin{aligned} P_s^{d_2} = & \frac{\xi^2 A}{24} \sum_{j=0}^{1} 3^j \sum_{i=1}^{N} \frac{\omega_i}{x_i} \left[\sum_{m=1}^{\beta} b_m \mathbf{G}_{1,3}^{3,0} \left(\frac{\left(\sqrt{3}/2\right)^j 2\sqrt{2}\alpha\beta\sigma_n x_i}{(g\beta+\Omega')\eta h_l A_0} \right) \right. \\ & \left. - \frac{\xi^2 A}{2} \times \sum_{m=1}^{\beta} \sum_{l=1}^{\beta} b_m b_l \mathbf{G}_{1,3}^{3,0} \left(\frac{\left(\sqrt{3}/2\right)^j 2\sqrt{2}\alpha\beta\sigma_n x_i}{(g\beta+\Omega')\eta h_l A_0} \right) \mathbf{G}_{2,4}^{3,1} \left(\frac{\left(\sqrt{3}/2\right)^j 2\sqrt{2}\alpha\beta\sigma_n x_l}{(g\beta+\Omega')\eta h_l A_0} \right) \right] \end{aligned} . \tag{15}$$

Next it is the turn to derive the $P_s^{d_5}$. Following the above definition, its integral form can be obtained as

$$P_s^{d_5} = \iint_{h_1<h_2<2h_1} Q\left(\frac{\sqrt{h_1^2+(h_2-h_1)^2}}{2\sigma_n}\right) f_h(h_1) f_h(h_2)\, dh_1 dh_2. \tag{16}$$

Due to the coupling of h_1 and h_2, it's impossible to convert the dual integral in Eq. 16 into two one-fold integrals. To further simplify Eq. 16, we employ the inequality approximation $\sqrt{a^2+b^2} \geq \frac{\sqrt{2}}{2}(a+b)$ to obtain $\sqrt{h_1^2+(h_2-h_1)^2} \geq \frac{\sqrt{2}}{2} h_2$,

$$P_s^{d_5} \approx \int_0^{+\infty} \left(\int_{h_2/2}^{h_2} f_h(h_1)\, dh_1 \right) \left[\frac{1}{12} e^{-\frac{\eta^2 h_2^2}{16\sigma_n^2}} + \frac{1}{4} e^{-\frac{\eta^2 h_2^2}{12\sigma_n^2}} \right] f_h(h_2) dh_2. \tag{17}$$

At this point, we find that $P_s^{d_5}$ has a similar form to Eqs. 8 and 14, which allows us to obtain its closed expression,

$$\begin{aligned} P_s^{d_5} = & \frac{\xi^4 A^2}{48} \sum_{j=0}^{1} 3^j \sum_{i=1}^{N} \frac{\omega_i}{x_i} \sum_{m=1}^{\beta} \sum_{l=1}^{\beta} b_l b_m \mathbf{G}_{1,3}^{3,0} \left(\frac{\left(\sqrt{3}/2\right)^j 4\alpha\beta\sigma_n x_i}{(g\beta+\Omega')\eta h_l A_0} \right) \\ & \times \left[\mathbf{G}_{2,4}^{3,1} \left(\frac{\left(\sqrt{3}/2\right)^j 4\alpha\beta\sigma_n x_i}{(g\beta+\Omega')\eta h_l A_0} \right) - \mathbf{G}_{2,4}^{3,1} \left(\frac{\left(\sqrt{3}/2\right)^j 2\alpha\beta\sigma_n x_i}{(g\beta+\Omega')\eta h_l A_0} \right) \right]. \end{aligned} \tag{18}$$

So far, we can obtain the final expression of SER P_s by substituting $P_s^{d_1}$, $P_s^{d_2}$, $P_s^{d_5}$ in Eqs. 13,15 and 17 into Eq. 7. The upper and lower bounds of 2 TXs' BER can be further obtained by substituting obtained P_s into Eq. 6.

Optics EXPRESS

3.3. Channel capacity

In this subsection, we will analyze the channel capacity of the UDC-FSO system. Different from the sum throughput defined in [15], which is defined as the information correctly transmitted per unit time, we define the channel capacity from the perspective of mutual information in this paper. Recalling that there are $|\mathbb{C}_m|$ possible codewords for the m-th TX's codebook, therefore there will be $N_M = \prod_{m=1}^{M} |\mathbb{C}_m|$ possible transmitting codewords and also N_M symbols after judgment process, i.e., $\psi_1, \ldots, \psi_{N_M}$. In other words, we should consider the discrete channel capacity C^{UDC} with N_M transmitting symbols and N_M received symbols. According to [22], the channel capacity can be shown as

$$C^{\mathrm{UDC}} = \frac{1}{n} \sum_{\psi_i \in \mathbf{\Psi}^{\mathbb{C}}} \sum_{\psi_j \in \mathbf{\Psi}^{\mathbb{C}}} p(\psi_i) \mathbf{P}(i,j) \log_2 \left[\frac{\mathbf{P}(i,j)}{\sum_{i=1}^{N_M} p(\psi_i) \mathbf{P}(i,j)} \right], \tag{19}$$

where $\mathbf{\Psi}^{\mathbb{C}} = \{\psi_i\}$ represents the sets of superimposed patterns. $\mathbf{P}$ is the transition probability matrix with the dimension of $N_M \times N_M$. The element $\mathbf{P}(i,j)$ in i-th row and j-th column means the conditional probability of the event that the correct superimposed pattern is ψ_i while it is judged into ψ_j by the receiver, i.e., $P(\psi_j|\psi_i)$. Obviously, $P(\psi_j|\psi_i)$ satisfies $\sum_i P(\psi_j|\psi_i) = 1$. $P(\psi_i)$ denotes the prior probability of ψ_i, which is equal to $1/N_M$.

Similarly, the discrete channel capacity of a legacy E2E link can be defined as

$$C^{\mathrm{E2E}} = \sum\nolimits_{i,j \in \{0,1\}} P(y=j, x=i) \log_2 \frac{P(x=i|y=j)}{p(x=i)}. \tag{20}$$

The channel capacity gain can be calculated by

$$\mathcal{G}_{\mathrm{UDC}} = C^{\mathrm{UDC}} / C^{\mathrm{E2E}}. \tag{21}$$

In large signal-to-noise ratio (SNR) cases, $\mathbf{P}$ will converge to a diagonal matrix. We can get

$$\lim_{SNR \to \infty} C^{\mathrm{UDC}} = \frac{1}{n} \log_2 N_M. \tag{22}$$

And for the E2E case, $\lim_{SNR\to\infty} C^{\mathrm{E2E}} = 1$. Thus $\lim_{SNR\to\infty} \mathcal{G}_{\mathrm{UDC}}$ converges to $\frac{1}{n}\log_2 N_M$.

4. Numerical results

To visually illustrate the effectiveness of the proposed MDSP, we simulate the above-mentioned 2 TXs and give the transfer probability matrix $\mathbf{P}$ in Fig. 4 for the three conditions $d_{\min} = d_1$, $d_{\min} = d_2$, and $d_{\min} = d_5$, respectively. It can be seen that the SER is dominated by the superimposed patterns related to d_1, d_2, d_5 in these three conditions, respectively. Not only that, as the SNR increases, the error events related to the distance $d_{\min}$ occur more often than the error probability corresponding to the other distances.

The SER performance is shown in Fig. 5, where the MDSP is valid in both strong and weak turbulence conditions for 2 TXs case (UDC-2, $\mathbb{C}_1 = \{[0,0],[1,1]\}$, $\mathbb{C}_2 = \{[0,1],[1,0],[0,0]\}$) and 3 TXs case(UDC-3, $\mathbb{C}_1 = \{[0,0],[1,1]\}$, $\mathbb{C}_2 = \{[0,1],[1,0]\}$, $\mathbb{C}_3 = \{[0,0],[1,0]\}$). During the simulation, the strong and weak turbulence conditions $(\alpha, \beta, g, \Omega')$ are set to $(4.2, 3, 0.4768, 2.0352)$ and $(8, 4, 0.02, 1)$ respectively [23,24]. The pointing error parameter A_0 is normalized to 1, and ξ is set to be 10. Moreover, the closed theoretical values derived in Sec.3.2 also coincide with the simulated values, where the Hermite order N is set to be 11. As with other NOMA techniques, the SER of the UDC-FSO system is worse than that of the conventional E2E link due to the non-orthogonal nature of the UDC, but it can lead to an increase in channel capacity [11]. It's also noted that the E2E link is equivalent to the baseline of the

Optics EXPRESS

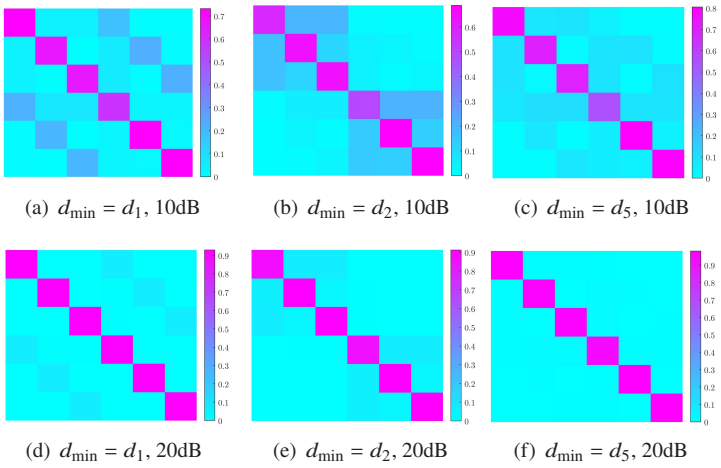

(a) $d_{\min} = d_1$, 10dB (b) $d_{\min} = d_2$, 10dB (c) $d_{\min} = d_5$, 10dB

(d) $d_{\min} = d_1$, 20dB (e) $d_{\min} = d_2$, 20dB (f) $d_{\min} = d_5$, 20dB

Fig. 4. Transition probability matrix $\mathbf{P}$ with $d_{\min} = d_1, d_2, d_5$.

orthogonal multiple access (OMA) situation with time division strategy, where only one TX is active in any arbitrary TS. In addition, the (255,239) Reed-Solomon (RS) coding is utilized as a comparison, which aims to show the difference of UDC and common forward error control (FEC) technique. As shown in Fig. 5, the SER curves with RS coding drop rapidly, which owes to the ability of correcting error symbols. Although both UDC and FEC belong to the "coding" perspective, they focus on different purposes, which are enhancing the effectiveness (increasing channel capacity) and improving the reliability (reducing BER), respectively.

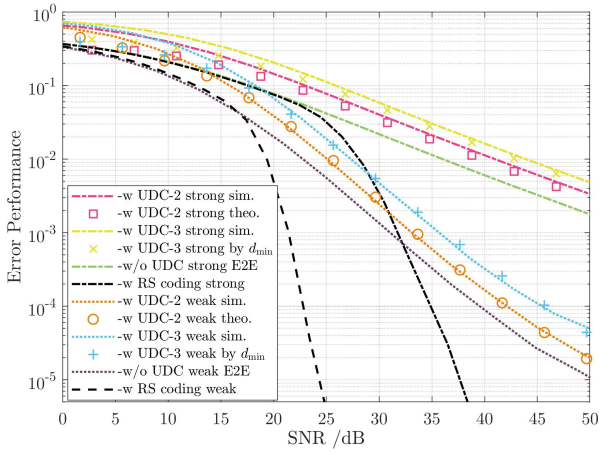

Fig. 5. SER of the UDC-FSO systems versus SNR.

The curves of the system BER with respect to its bounds are given in Fig. 6 for different channel fluctuations, where the 2 TXs case is depicted in Fig. 6(a) and the 3 TXs condition is given in Fig. 6(b). It can be seen from Fig. 6 that the BER curves can be completely covered by the bounds, which also verifies the conclusion of Eq. 6. It needs to mention that the BER curves in in Fig. 6 are achieved by simulation results. When acquiring the bounds, we first simulate the SER, and then derive the bounds (P_s and $P_s/\log_2 N_M$) according to the obtained P_s and N_M.

The channel capacity C^{UDC} and channel capacity gain $\mathcal{G}_{\mathrm{UDC}}$ of the UDC-FSO system are given in Fig. 7, respectively. It's observed that C^{UDC} converges to $\frac{1}{2}\log_2 6 = 1.2925$ bit/symbol

Optics EXPRESS

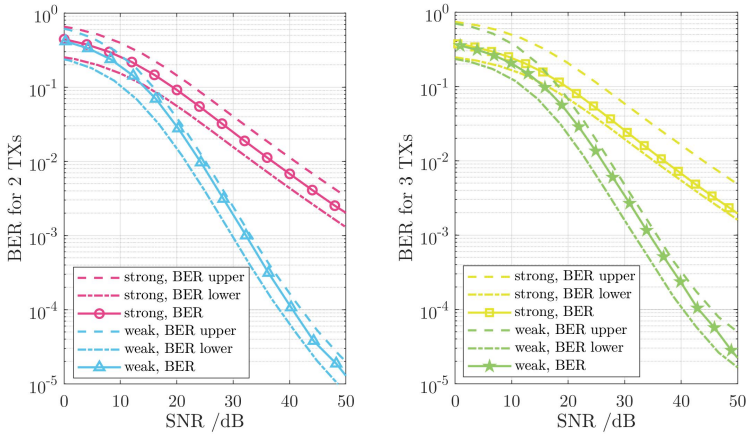

(a) 2 TXs case (b) 3 TXs case

Fig. 6. BER and BER's bounds for UDC-FSO systems.

($\frac{1}{2}\log_2 8 = 1.5$ bit/symbol) for the condition of 2 TXs (3 TXs) under the large SNR circumstances. The results in Fig. 7 also verify the statement of $\lim_{SNR\to\infty} C^{\mathrm{UDC}} = \frac{1}{n}\log_2 N_M$ in Sec.3.3, which indicates that the upper limit of channel capacity of the UDC-FSO system is only affected by the set of UDC codewords. Therefore the UDC-FSO system can be optimized from the perspective of constructing codewords. As obtained from Fig. 7(a), the channel capacity with RS coding will converge at 239/255 (the code rate for channel coding), which is smaller than a unit quantity. It's concluded from Figs. 5 and 7 that the traditional FEC technique has the ability of reducing SER. However, it does not only contribute positively to improving the channel capacity bound, but reduces the upper bound of channel capacity under high SNR conditions due to the redundancy it introduces for the correcting errors. Moreover, it's also discovered from Fig. 7 that the channel capacity of UDC-FSO system is constantly larger than both the E2E link and the RS coding scheme under the same channel conditions, which demonstrates the superiority of UDC-FSO.

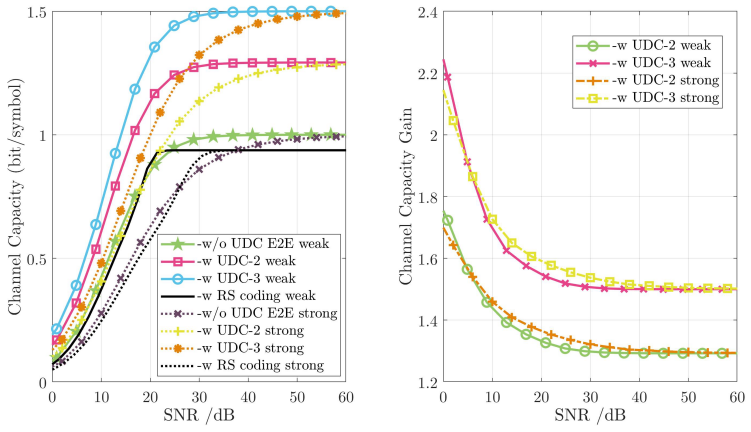

(a) C^{UDC} and C^{E2E} (b) $\mathcal{G}^{\mathrm{UDC}}$

Fig. 7. Channel capacity and channel capacity gain of the UDC-FSO systems versus SNR.

Figure 8 shows both the SER (left axis) and channel capacity (right axis) of a UDC-FSO system with strong turbulence versus different pointing error parameter ξ, where the SNR are

Optics EXPRESS

assumed to be 30, 40 and 50dB. It's seen that the SER performs better with increasing ξ, which can be explained by the reason that larger ξ corresponds to the condition of smaller pointing error displacement standard deviation with certain receiver's equivalent beam radius. The channel capacity curve can be interpreted according to the same reasoning.

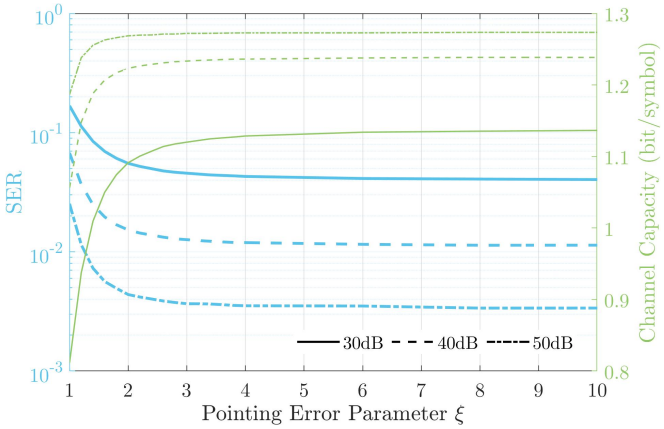

Fig. 8. SER (left axis) and channel capacity (right axis) of a UDC-FSO system with different pointing error parameter ξ.

It needs to mention that the PD-NOMA is not given as comparison curves. The four main reasons are as follows. I) In the field of optical communication, most PD-NOMA literatures focus on the VLC systems [25,26], while this paper is based on FSO systems. Both transceivers and channel models are different. II) OFDM technique is always utilized in PD-NOMA VLC systems, while this paper considers the OOK scheme. Different modulation methods cause the difficulty of fair comparison. III) Although [12] studies the performance of PD-NOMA in an analog OOK VLC system, its signal expression is different from this paper $\mathbf{y}^k = \eta \sum_{m=1}^{M} h_m^k \cdot \mathbf{c}_m^k + \mathbf{n}^k$. Instead, its signal expression is ($y_k = \gamma h_k \sum_{i=1}^{N} P_i s_i + n_k$). The difference is that the signal in this paper is superimposed after passing through different channels, while [12] assumes that the signal is superimposed and then passes through the channel. IV) According to [27], the current studies on PD-NOMA and CD-SCMA are mostly carried out in a disjoint manner and little have been understood on their performance comparison. In other words, a fair comparison of these two systems in terms of their performance is a broad subject to be studied, which is beyond this paper.

Next, we set up an equivalent desktop experiment with 2 TXs, shown in Fig. 9. Ch1 and Ch2 of the Arbitrary Wave Generator (AWG, Tektronix AWG70002A) transmit the UDC-encoded electrical signal which is connected to the electro-optical modulator and attenuator. After receiving lens couples the combined signals from TX-1 and TX-2 into the fiber. The photodiode (PD, New Focus 1592) outputs the converted electrical signal which is further collected and stored by an oscilloscope (Tektronix, DPO7354) for post-processing.

Figure 10 depict the probability of $P(\psi_j|\psi_i), i \neq j$ for the three cases $d_{\min} = d_1, d_2$, and d_5, respectively. Taking $d_{\min} = d_1$ in Fig. 10 as an example ($h_2/h_1 = 0.6935$ satisfying $h_2 < h_1$), it's obtained that the superimposed patterns with distance of d_1 (i,e, $\psi_1 \leftrightarrow \psi_2$, $\psi_1 \leftrightarrow \psi_3$, $\psi_4 \leftrightarrow \psi_5$, and $\psi_4 \leftrightarrow \psi_6$) have much higher error probability than the other patterns. The corresponding average SER is 2.35×10^{-4}. The average BER is equal to 1.46×10^{-4}, which lies in the bounds $[9.09 \times 10^{-5}, 2.35 \times 10^{-4}]$. The channel capacity is 1.2908 bit/symbol. Similar conclusions can be drawn in Fig. 10 ($h_2/h_1 = 1.442$) and Fig. 10 ($h_2/h_1 = 2.5833$) for $d_{\min} = d_2$, $d_{\min} = d_5$ cases, respectively, where the average SERs are 2.37×10^{-5} and 2.4×10^{-3}, and the BER is 2.35×10^{-5} and 9.55×10^{-4}, respectively. It's also observed that the BERs of the latter two cases are still in the ranges $[9.17 \times 10^{-6}, 2.37 \times 10^{-5}]$ and $[9.28 \times 10^{-4}, 2.4 \times 10^{-3}]$. Although the BER belongs

Optics EXPRESS

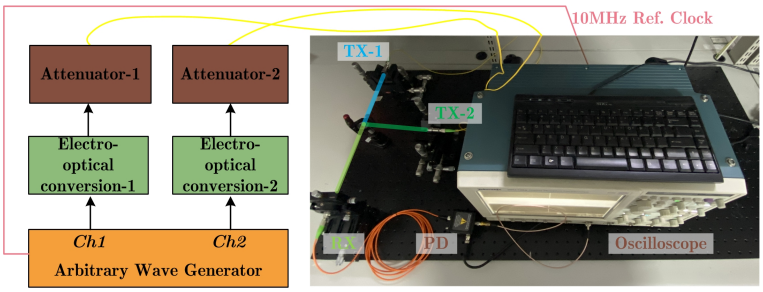

Fig. 9. Equivalent experimental scene and structure diagram.

to the bound regions in all the three cases $d_{\min} = d_1, d_2, d_5$, the relative distances from the bounds are different with respect to different candidates of $d_{\min}$. It's indicated that the UDC codebook $\mathbb{C}$ has an influence on the BER results, due to $\mathbb{C}$ determines the candidates of $d_{\min}$. The channel capacities of the latter two cases are 1.2923 bit/symbol and 1.2802 bit/symbol, respectively.

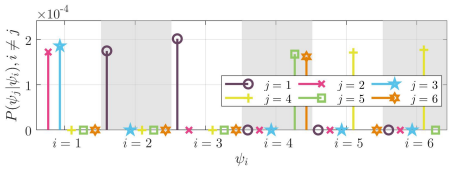

(a) $d_{\min} = d_1$

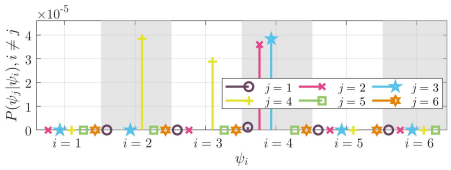

(b) $d_{\min} = d_2$

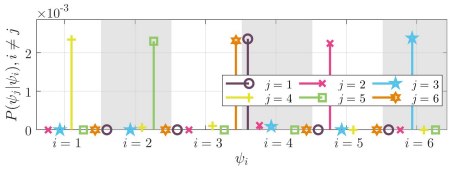

(c) $d_{\min} = d_5$

Fig. 10. Error performance of experimental results.

It's also concluded from the experiments that the proposed MDSP approximation method is effective. Consequently, $d_{\min}$ of the set of superimposed patterns is the decisive factor affecting the SER and channel capacity in the UDC-FSO system. As a result, the system metrics can be optimized by maximizing $d_{\min}$. Since $d_{\min}$ is influenced by both the discrete codeword space and continuous channel space, the performance of the UDC-FSO system can be further optimized by codeword construction and power allocation.

Optics EXPRESS

5. Conclusion

In this paper, a quantitative analysis of the UDC-FSO system is carried out, where both Malaga turbulence and pointing errors are considered. Considering that the variety of UDC codeword sets can lead to more complex region division, it is impossible to apply the region integration method commonly used in soft judgment methods when deriving SER. To solve the difficulties of multi-integrations in irregular regions, the MDSP approximation method is first proposed, which is verified by experiments. Based on the MDSP, the universal SER of a UDC-FSO system can be deduced approximately. The deduced universal SER is verified in the case of 2 TXs case and 3 TXs case. And taking 2 TXs as an example ($\mathbb{C}_1 = \{[0,0],[1,1]\}, \mathbb{C}_2 = \{[0,1],[1,0],[0,0]\}$), the closed expression of SER is derived, which is further verified by simulation. On the basis of SER, both the upper and lower bounds of BER are analyzed. Based on the transition probability matrix of superposition patterns, we define and calculate the discrete channel capacity of a UDC-FSO system from the point of the information theory, which is more universal than the throughput discussed in our previous work [15]. It's also revealed that the maximum value of channel capacity of UDC-FSO system is $1/n\log_2 N_M$, which means that the UDC codewords determine the performance of a UDC-FSO system. Moreover, through simulation and equivalent desktop experiments, it is verified that the minimum distance $d_{\min}$ of the superimposed patterns is the core factor affecting the SER, and thus the channel capacity. It's a possible solution to optimize UDC-FSO systems by maximizing $d_{\min}$ through power allocation or UDC codebook construction.

Appendix A

In this appendix, the proof for **REMARK** 1 will be presented. Since there are N_M superimposed patterns, the SER can be written in the form of Eq. A1,

$$P_s = \sum_{i=1}^{N_M} \sum_{\substack{j=1 \\ j\neq i}}^{N_M} P(\psi_i) P\left(\psi_j \,|\psi_i\right), \tag{A1}$$

where $P\left(\psi_j \,|\psi_i\right) = \int_{\mathcal{S}_j} p\left(\mathbf{y} \,|\psi_i\right) d\mathbf{y}$. $\mathcal{S}_j$ stands for the judgement region of ψ_j. We also define $\mathcal{S}$ as the n-dimensional hyperplane where the receiving symbol $\mathbf{y}$ belongs. $\bar{\mathcal{S}}_j$ is defined as the judgment region except ψ_j, which means $\bar{\mathcal{S}}_i = \mathcal{S}$ - $\mathcal{S}_j = \sum_{i\neq j} \mathcal{S}_i$. As a result, Eq. A1 turns to

$$P_s = \frac{1}{M} \sum_{i=1}^{N_M} \sum_{\substack{j=1 \\ j\neq i}}^{N_M} \int_{\mathcal{S}_j} p\left(\mathbf{y} \,|\psi_i\right) d\mathbf{y} = \frac{1}{M} \sum_{i=1}^{N_M} \underbrace{\int_{\bar{\mathcal{S}}_i} p\left(\mathbf{y} \,|\psi_i\right) d\mathbf{y}}_{P_{s|\psi_i}}, \tag{A2}$$

where $P_{s|\psi_i}$ denotes the The conditional SER when the transmitted superimposed pattern is ψ_i. For any superimposed pattern ψ_i, $P_{s|\psi_i}$ can be approximated as the pairwise error probability between itself and its closest superimposed pattern, i.e., $P_{s|\psi_i} \approx \mathbb{E}\left[Q\left(\frac{d^i_{\min}}{2\sigma_n}\right)\right]$, where $d^i_{\min}$ represents the minimal distance between ψ_i and its closest superimposed pattern. In the sequel, we can have the final approximation by

$$P_s \approx \frac{1}{M} \sum_{i=1}^{N_M} \mathbb{E}\left[Q\left(\frac{d^i_{\min}}{2\sigma_n}\right)\right] \approx \frac{1}{M} \sum_{i=1}^{N_M} \mathbb{E}\left[Q\left(\frac{d_{\min}}{2\sigma_n}\right)\right] = \mathbb{E}\left[Q\left(\frac{d_{\min}}{2\sigma_n}\right)\right]. \tag{A3}$$

So far, **REMARK** 1 has been proved. ■

Funding. National Natural Science Foundation of China (62101527); Funding Program of Innovation Labs by Changchun Institute of Optics, Fine Mechanics and Physics, Chinese Academy of Sciences (Y9J132E).

Optics EXPRESS

Disclosures. The authors declare no conflicts of interest.

Data availability. Data underlying the results presented in this paper are not publicly available at this time but may be obtained from the authors upon reasonable request.

References

1. A. Trichili, M. A. Cox, B. S. Ooi, and M.-S. Alouini, "Roadmap to free space optics," J. Opt. Soc. Am. B **37**(11), A184 (2020).
2. R. Samy, H. -C. Yang, T. Rakia, and M. -S. Alouini, "Space-Air-Ground FSO Networks for High-Throughput Satellite Communications," IEEE Commun. Mag. **61**(3), 82–87 (2023).
3. J. Li, Y. Yuan, and Y. Cai, "High-precision clock date recovery for optical wireless communications using orbital-angular-momentum-based mode division multiplexing," Opt. Lett. **48**(11), 3107–3110 (2023).
4. C. M. Schieler, K. M. Riesing, A. J. Horvath, B. C. Bilyeu, J. S. Chang, A. S. Garg, J. P. Wang, and B. S. Robinson, "200 Gbps TBIRD CubeSat downlink: pre-flight test results," Proc. SPIE, Free-Space Laser Communications XXXIV **119930**, 34 (2022).
5. H. Cui, J. Zhang, Y. Geng, Z. Xiao, T. Sun, N. Zhang, J. Liu, Q. Wu, and X. Cao, "Space-Air-Ground Integrated Network (SAGIN) for 6G: Requirements, Architecture and Challenges," China Commun. **19**(2), 90–108 (2022).
6. R. Zhang, "Full-duplex hybrid optical link with 40 Gbit/s 16-QAM signal for wired or wireless selective access based on polarization division multiplexing," Appl. Opt. **61**(14), 4005–4012 (2022).
7. X. Weng, B. Muminov, and L. T. Vuong, "Diffractal Spatial Multiplexing for Free-space Communication with Roving Transceivers," Proc. Frontiers in Optics Laser Science, FTh5E.5 (2020).
8. S. Zhu, P. Qiu, X. I Shan, R. Lin, Z. Wang, Z. Jin, X. Cui, G. Zhang, and P. Tian., "High-speed long-distance visible light communication based on multicolor series connection micro-LEDs and wavelength division multiplexing," Photonics Res. **10**(8), 1892 (2022).
9. J. Du, W. Shen, J. Liu, Y. Chen, X. Chen, and Z. He, "Mode division multiplexing: from photonic integration to optical fiber transmission," Chin. Opt. Lett. **19**(9), 091301 (2021).
10. W. H. Gunawan, Y. Liu, C.-W. Chow, Y.-H. Chang, C.-W. Peng, and C.-H. Yeh, "Two-Level Laser Diode Color-Shift-Keying Orthogonal-Frequency-Division-Multiplexing (LD-CSK-OFDM) for Optical Wireless Communications (OWC)," J. Lightwave Technol. **39**(10), 3088–3094 (2021).
11. X. Zhang, D. Zhang, L. Yang, G. Han, H. -H. Chen, and D. Zhang, "SCMA Codebook Design Based on Uniquely Decomposable Constellation Groups," IEEE Trans. Wireless Commun. **20**(8), 4828–4842 (2021).
12. C. Chen, W. -D. Zhong, H. Yang, and P. Du, "On the Performance of MIMO-NOMA-Based Visible Light Communication Systems," IEEE Photon. Technol. Lett. **30**(4), 307–310 (2018).
13. Q. Yu and K. Song, "Uniquely Decodable Multi-Amplitude Sequence for Grant-Free Multiple-Access Adder Channels," IEEE Trans. Wireless Commun. (2023).
14. M. Kulhandjian, H. Kulhandjian, C. D' Amours, H. Yanikomeroglu, D. A. Pados, and G. Khachatrian, "Low-Complexity Decoder for Overloaded Uniquely Decodable Synchronous CDMA," IEEE Access **10**, 46255–46275 (2022).
15. Y. Li, T. Geng, and S. Gao., "Improve the throughput of M-to-1 free-space optical systems by employing uniquely decodable codes," Chin. Opt. Lett. **21**(3), 030603 (2023).
16. M. Kulhandjian, H. Kulhandjian, and C. D' Amours, "Uniquely Decodable Ternary Codes via Augmented Sylvester-Hadamard Matrices," BlackSeaCom 1–6 (IEEE, 2021).
17. S. Lu, W. Hou, J. Cheng, and H. Kamabe, "Recursive Construction of k-Ary Uniquely Decodable Codes for Multiple-Access Adder Channel," ISITA, 565-569 (IEEE, 2018).
18. H. Wu, D. Kang, J. Ding, J. Yang, Q. Wang, J. Wu, and J. Ma, "Secrecy performance analysis in the FSO communication system considering different eavesdropping scenarios," Opt. Express **30**(23), 41028 (2022).
19. A. Das, B. Bag, C. Bose, and A. Chandra, "Performance analysis of FSO links employing a transmit and receive diversity-based operating system under Málaga turbulence channels with pointing errors," Opt. Continuum **1**(2), 366 (2022).
20. W. Gappmair, S. Hranilovic, and E. Leitgeb, "Performance of PPM on terrestrial FSO links with turbulence and pointing errors," IEEE Commun. Lett. **14**(5), 468–470 (2010).
21. X. Wang, GitHub repository, https://github.com/pillowlab/GaussHermiteQuadrature.
22. T. Cover and J. Thomas, *Elements of Information Theory*, 2nd ed. (Wiley, 2006).
23. I. S. Ansari, F. Yilmaz, and M. -S. Alouini, "Performance Analysis of Free-Space Optical Links Over Malaga (M) Turbulence Channels With Pointing Errors," IEEE Trans. Wireless Commun. **15**(1), 91–102 (2016).
24. E. Balti, M. Guizani, B. Hamdaoui, and B. Khalfi, "Aggregate Hardware Impairments Over Mixed RF/FSO Relaying Systems With Outdated CSI," IEEE Trans. Commun. **66**(3), 1110–1123 (2018).
25. Z. Wang, L. Zhang, J. Li, G. Wei, Y. Dong, and H. Y. Fu, "Fluorescent concentrator based MISO-NOMA for visible light communications," Opt. Lett. **47**(4), 902–905 (2022).
26. V. Dixit and A. Kumar, "Error analysis of L-PPM modulated MIMO based multi-user NOMA-VLC system with perfect and imperfect SIC," Appl. Opt. **61**(4), 858 (2022).
27. Q. Luo, P. Gao, and Z. Liu, "An Error Rate Comparison of Power Domain Non-Orthogonal Multiple Access and Sparse Code Multiple Access," IEEE Open J. Commun. Soc. **2**, 500–511 (2021).